Biology of Reproduction, 2022, **106(1)**, 132–144
https://doi.org/10.1093/biolre/ioab217
Advance access publication date 26 November 2021
Research Article

Dynamics of epigenetic modifiers and environmentally sensitive proteins in a reptile with temperature induced sex reversal†

Sarah L. Whiteley[1,2], Robert D. McCuaig[3], Clare E. Holleley[2], Sudha Rao[3] and Arthur Georges[1,*]

[1]Faculty of Science and Technology, Institute for Applied Ecology, University of Canberra, Canberra, Australia
[2]Australian National Wildlife Collection CSIRO National Research Collections Australia, Canberra, Australia
[3]Gene Regulation and Translational Medicine Laboratory, QIMR Berghofer Medical Research Institute, Brisbane, Australia

***Correspondence**: Faculty of Science and Technology, Institute for Applied Ecology, University of Canberra ACT 2617, Building 3, Kirinari Street, Canberra, Australia. Tel: +61418866741; E-mail: georges@aerg.canberra.edu.au

†**Grant Support:** Funding for this project was provided by a Discovery Grant from the Australian Research Council (DP170101147) awarded to A.G. (lead), C.E.H., Janine Deakin, Tariq Ezaz, Stephen Sarre, Lisa Schwanz, Paul Waters, and Jennifer Marshall Graves. Additional funding was provided by a CSIRO Research Plus Postgraduate Award awarded to S.L.W.

Abstract

The mechanisms by which sex is determined, and how a sexual phenotype is stably maintained during adulthood, have been the focus of vigorous scientific inquiry. Resources common to the biomedical field (automated staining and imaging platforms) were leveraged to provide the first immunofluorescent data for a reptile species with temperature induced sex reversal. Two four-plex immunofluorescent panels were explored across three sex classes (sex reversed ZZf females, normal ZWf females, and normal ZZm males). One panel was stained for chromatin remodeling genes JARID2 and KDM6B, and methylation marks H3K27me3, and H3K4me3 (Jumonji Panel). The other CaRe panel stained for environmental response genes CIRBP and RelA, and H3K27me3 and H3K4me3. Our study characterized tissue specific expression and cellular localization patterns of these proteins and histone marks, providing new insights to the molecular characteristics of adult gonads in a dragon lizard *Pogona vitticeps*. The confirmation that mammalian antibodies cross react in *P. vitticeps* paves the way for experiments that can take advantage of this new immunohistochemical resource to gain a new understanding of the role of these proteins during embryonic development, and most importantly for *P. vitticeps*, the molecular underpinnings of sex reversal.

Summary sentence
Immunostaining of important chromatin modifiers, histone marks, and environmental response proteins across the three functional sexes in *Pogona vitticeps* shows protein dynamics differ between males, females, and sex reversed females.

Keywords: fluorescent immunostainingi, mmunohistochemistry, gonad proteins, gonad morphology, protein expression

Introduction

The phenotypic sex of an animal governs many aspects of their life history and their reproductive success. The mechanisms by which sex is determined, and how a sexual phenotype is stably maintained during adulthood, have been the focus of vigorous scientific inquiry. Across vertebrates, sex is determined by a variety of mechanisms that exist on a spectrum between genetic sex determination (GSD) and environmental sex determination (ESD). In GSD systems, sex is controlled by genes on sex chromosomes, whereas ESD systems sex determination is flexible and sensitive to a wide variety of environmental stimuli. Although species typically possess one system or the other, but discovery of species with sex governed by gene–environment interactions is increasing [1]. Examples of such species are few and poorly characterized [2]. An exception is the emerging model organism, the central bearded dragon (*Pogona vitticeps*). *Pogona vitticeps* has sex microchromosomes (female heterogamety, ZZ/ZW; [3]), however their influence can be overridden by high incubation temperatures (>32°C) in ZZ males [4]. This triggers sex reversal, so that ZZ males develop as phenotypic females. As such, this species possesses a sex determination system ideally suited to studying the influences of both sex chromosomes and the environment on sex. Sex reversed ZZf females differ from concordant ZWf females in several biological aspects, including karyotype, behavior, morphology, reproduction, and gene expression [5–7], though the two female sex classes do not differ in bite force [8].

Molecular resources supporting the study of sex differences in *P. vitticeps* are increasing [7, 9–11], but much remains to be characterized. For example, little is known about the adult gonadal phenotypes in *P. vitticeps*, and nothing is known about protein expression or localization (see [12–16] for protein expression in other reptile species). To better understand protein dynamics of adult gonads of *P. vitticeps*, we selected for immunofluorescence analysis, a series of chromatin modifiers, their target methylation marks and environmentally sensitive regulators, all of which have been implicated in sex determination and sex reversal in *P. vitticeps* and reptiles more broadly [7, 17–19]. These include chromatin remodeling genes

Received: August 12, 2021. **Revised:** October 25, 2021. **Editorial decision:** November 16, 2021

JARID2 (Jumonji and AT-rich domain containing 2) and KDM6B (lysine demethylase 6B, also known as JMJD3) both of which regulate the methylation status of lysine 27 on histone 3 (H3K27). JARID2 is part of PRC2 (polycomb remodeling complex 2), which methylates H3K27 to H3K27me3, whereas KDM6B has an opposing function that activates gene expression by demethylating H3K27me3 [20, 21]. Other members of the Jumonji gene family, such as JMJD1C, have roles in germ cell regulation in mammalian gonads [22, 23]. The co-occurrence of H3K27me3 repressive marks with active H3K4me3 marks is characteristic of bivalent chromatin. This pattern of epigenetic modification is commonly present during germ cell proliferation in mammalian gonads [24, 25]. However, the dynamics of bivalent chromatin in reptiles is completely unknown.

Genes with environmental sensitivity are of particular interest for many reptile species, including *P. vitticeps*, because they might play a role in regulating environmentally triggered sex determination. CIRBP (cold inducible RNA binding protein) is of particular interest as a regulator of temperature sex reversal in *P. vitticeps* and in temperature sex determination in turtles [7, 26, 27]. It is not known if the expression of CIRPB in TSD species directs sexual phenotypes only during development, if it is also required to maintain adult gonadal cellular identity, or if it performs some other function. For example, in mammalian gonads CIRBP is involved in cell protection against environmental stressors [28, 29]. Thus, to further explore the importance of cell protection in the context of CIRPB expression, we selected a member of the NF-κB cell signaling pathway that mediates inflammatory and immune responses for further study. Specifically, RelA/p65 has well established roles in initiating cell protective responses in the gonad in response to the environment [30–33]. A recent model for the mechanisms of temperature response in environmentally sensitive species suggests an important role for the NF-κB and its signaling participants, like RelA. Currently nothing is known about the role of RelA in reptile gonads, and little is known about its functions in mammalian gonads [33], warranting further exploration of the activities of RelA in gonads.

Although protein expression and localization in mammalian gonads is extensively studied, research in non-mammalian species, particularly reptiles, is lacking by comparison. To determine the protein profiles of adult gonads in *P. vitticeps*, antibodies raised in mammals against mammalian targets were used in *P. vitticeps* for the first time to determine if they cross-react in a reptile. Resources common to the biomedical field (automated staining and imaging platforms) were leveraged to provide the first immunofluorescent data for this species. Two four-plex immunofluorescent panels were explored across the three sex classes (sex reversed ZZf and concordant ZWf females, and ZZm males). The first panel termed the Jumonji panel stained for JARID2, KDM6B, H3K27me3, and H3K4me3. The second, called the CaRe panel after a model that implicates two of the targets in this panel in sex reversal [34], stained for CIRBP, RelA, H3K27me3, and H3K4me3. Our study characterizes tissue specific expression and cellular localization patterns of these proteins and histone marks, providing new insights to the molecular characteristics of adult gonads in *P. vitticeps*.

Materials and methods

Sample collection and histology

All adult animals (Table 1) were obtained from the breeding colony at the University of Canberra, Australia. All animals were humanely euthanized at the end of the 2017–18 breeding season (September–March) via an intravenous injection of sodium pentobarbitone (60 mg/ml in isotonic saline) in accordance with approved animal ethics procedures at the University of Canberra (UC AEC 0270). Animals were selected on the basis of their genotypic sex using an established PCR test [6], and the gonadal phenotype was confirmed upon dissection. Sex reversed females were obtained by laboratory incubations at 36°C, as these incubation temperatures induce sex reversal (96% rate of reversal; [6]). Gonads were dissected immediately following euthanasia and preserved in 4% PFA-PBS. All initial tissue processing stages (tissue dehydration, wax embedding, and serial sectioning) was conducted at the University of Queensland's School of Biomedical Sciences Histology facility. Samples were processed according to standard protocols, sectioned 3-μm thick, and placed on positively charged microscope slides.

Additional hematoxylin and eosin staining was conducted on representative slides for each of the three sex classes (ZZf and ZWf females, and ZZm males) by QIMR's Histology Services for ease of cell type identification (Supplementary Figure S1).

Immunohistochemistry

For immunofluorescent staining, antibodies for the targets of interest (Table 2) were selected based on high homology with the region against which the antibody was raised. Antibodies with sequence homology to *P. vitticeps* >85% were considered for subsequent testing and optimization. All antibodies selected had undergone validation by the supplier to cross-react in mammals and to be suitable for immunofluorescence of formalin-fixed paraffin-embedded (FFPE) tissues.

Each antibody was first optimized via serial dilutions, and then each multiplex panel was optimized for staining intensity and specificity (Table 2). All staining procedures were conducted using the Opal Polaris 4 color Automation Kit (Perkin Elmer, cat no. NEL810001KT) optimized for use on the Leica Bond RX Automated IHC Research Stainer (Leica Biosystems). To ensure staining was specific for primary antibodies all appropriate negative controls for staining were employed for the Jumonji and CaRe panels. This included primary antibody only controls (with no secondary detection), secondary detection controls (with no primary antibodies) and blank controls with no staining protocol (see Supplementary Figure S2).

Image analysis and quantification

Formalin-fixed paraffin-embedded sections (3 μM thick) from *P. vitticeps* of gonadal tissue sections of three individuals from each sex class in *P. vitticeps* (sex reversed ZZf and concordant ZWf females, and ZZm males) were stained with multiplex immunohistochemistry (IHC) Jumonji panel of four targets (H3K27me3, H3K4me3, JARID2, and KDM6B) following single stain optimization. A subset of samples (two from each sex class) were stained with the CaRe multiplex panel (H3K27me3, H3K4me3, CIRBP, and RelA). Although H3K27me3 and H3K4me3 were stained between both panels,

Table 1. Specimen identification numbers and genotypic and phenotypic sex of all adult *Pogona vitticeps* used in this study

Specimen ID	Sex class	Genotypic sex	Phenotypic sex
005005003424	Concordant Female	ZW	Ovaries
111880109533	Concordant Female	ZW	Ovaries
005005003551	Concordant Female	ZW	Ovaries
005005003596	Sex reversed female	ZZ	Ovaries
111880108006	Sex reversed female	ZZ	Ovaries
005005003388	Sex reversed female	ZZ	Ovaries
111880108027	Concordant Male	ZZ	Testes
111880109557	Concordant Male	ZZ	Testes
111880108009	Concordant Male	ZZ	Testes

Table 2. Details of antibody targets used in this study, including their origin species and clonality, the company and catalogue number, serial and final dilutions used for each antibody, and the biological function of each target

Target name	Type (origin species, clonality)	Company (catalogue number)	Serial dilutions	Final dilution	Function
H3K27me3 (tri-methyl lysine 27)	Mouse monoclonal	Abcam (ab6002)	1/100, 1/200, 1/400, 1/800	1/200	Methylation marks associated with transcriptional silencing deposited by the PRC2 complex
H3K4me3 (tri-methyl lysine 4)	Rabbit polyclonal	Abcam (ab8580)	1/100, 1/200, 1/400, 1/800	1/200	Methylation marks associated with active gene expression
JARID2	Rabbit polyclonal	Abcam (ab213679)	1/50, 1/100, 1/200, 1/400	1/100	Component of the PRC2 complex. Intron retention event in sex reversed females
JMJD3/KDM6B	Rabbit polyclonal	Genetex (GTX124222)	1/50, 1/100, 1/200, 1/400	1/100	Demethylase for H3K27me3 (antagonist to PRC2)
RelA (p65)	Mouse monoclonal	Santa Cruz Biotechnology (sc-68008)	1/50, 1/100, 1/200, 1/400	1/100	Component of the NF-kB pathway
CIRBP (cold-inducible binding protein)	Mouse monoclonal	Santa Cruz Biotechnology (sc-293325)	1/50, 1/100, 1/200, 1/400	1/100	Induced by environmental cues, identified as key gene in TSD pathways

any subsequent analysis was conducted in a panel-specific manner, and comparisons of the staining of these two targets between the two panels were not made as these results would be influence by technical variation that is not biologically relevant.

The slides were imaged using the ASI Digital Pathology System. Touching cells were automatically segmented, signal expression was quantitatively measured, and results per cell and over the entire scanned region displayed. For high-throughput microscopy, protein targets were localized by confocal laser scanning microscopy. Single 0.5-μm sections were obtained using an Olympus-ASI automated microscope with a 100× oil immersion lens running ASI software. The final image was obtained by employing a high-throughput automated stage with ASI spectral capture software [35, 36]. Digital images were analyzed using automated ASI software (Applied Spectral Imaging, Carlsbad, CA) to automatically determine the distribution and immunofluorescent intensities with automatic thresholding and background correction of the mean integrated fluorescent intensity (MIFI, described below). Images were prepared for representative purposes using ImageJ Fiji imaging software [37].

Mean integrated fluorescent intensity values detected by the ASI automated software platform were obtained by normalizing the fluorescent signal from each target for the area of each cell. Cells were classified into different classes depending on whether they expressed a single target, or multiple targets, yielding 10 classes of cells in which one or more target was present. A minimum of three cells within a given sex class needed to have the cell class detected to be used for the analysis. Global levels of expression for each of the four targets were determined by combining the MIFI of all classes that had positive staining for each target. The ASI automated software only detects and measures the fluorescent signal originating from within a cell, so that any background staining does not influence the MIFI values obtained for the targets.

The MIFI values for each class were normalized via log transformation, and statistical differences of these values between the three sex classes was assessed using a linear model (lm function) in R (version 1.2.1335). Global expression of each target was obtained by summing the values for the given target in each class in which it was detected. All graphs were prepared in R using the ggplot2 package [38].

Results

Ovarian morphology

The morphological characteristics of *P. vitticeps* ovarian follicles in both ZZf discordant sex reversed adult females and

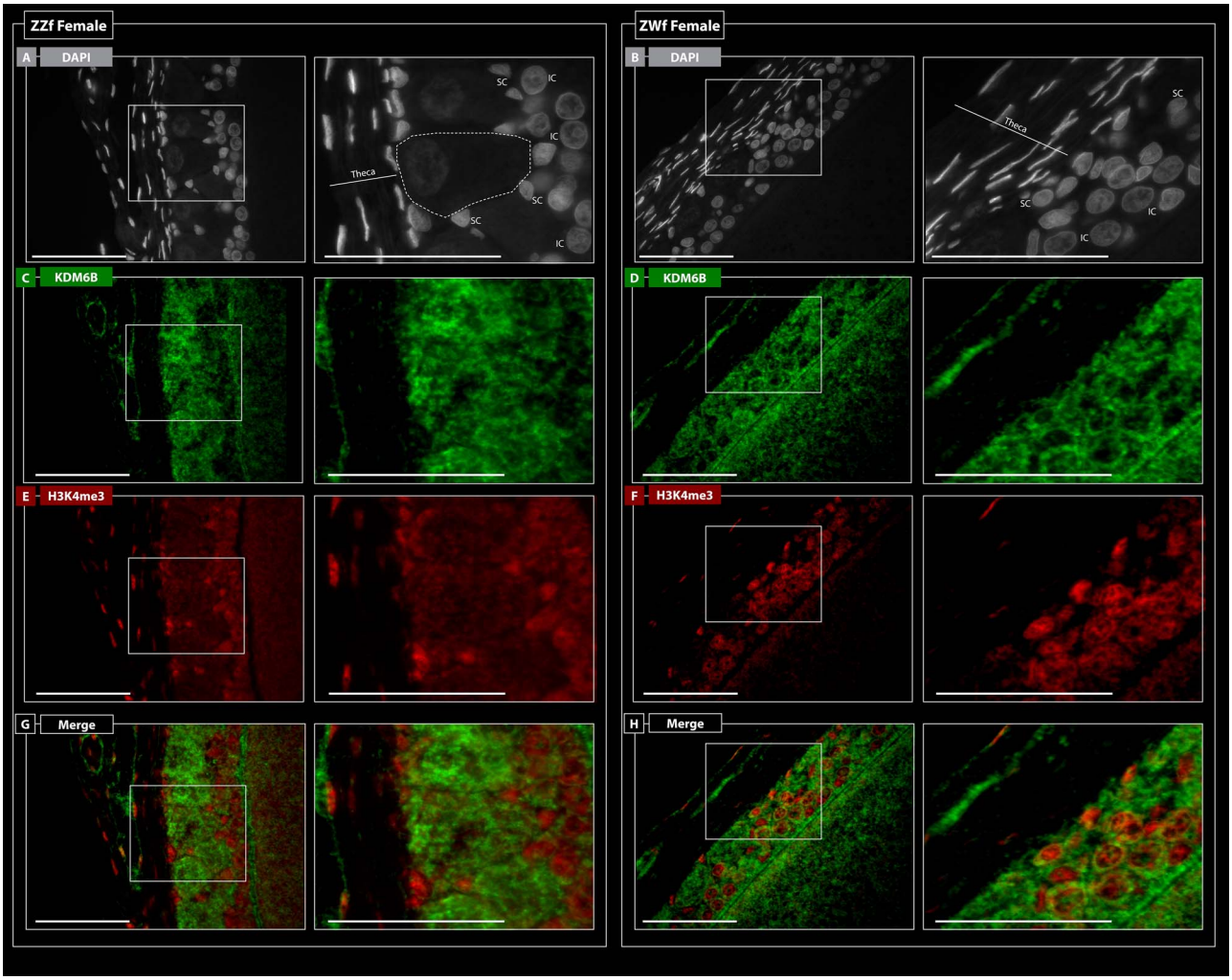

Figure 1. Immunofluorescence of KDM6B (green) and H3K4me3 (red) in adult ZZf sex reversed ovaries (panels A, C, E, and G) and ZWf concordant (panels B, D, F, and H) ovaries at 100× magnification. Panels G and H show a merged image of KDM6B and H3K4me3 staining. A pyriform cell in the ZZf female in panel A is demarcated by a dotted white outline. The white boxes indicate the portion of the image that has been zoomed in. SC = small cells, IC = intermediate cells. Scale bar = 10 μm.

ZWf concordant females during the previtellogenesis phase are aligned with what has been previously published in reptiles [39–42]. In ZZf females the granulosa layer has become stratified and contains small, intermediate, and pyriform cell types [40]. The zona pellucida is present as a single layer between the granulosa and the developing ooplasm. Small cells are spherical with round nuclei that are closest to the theca and interspersed among the pyriform cells. The intermediate cells are oval with a round nucleus and are prevalent in the contact region with the ooplasm. The pyriform cells have large nuclei and a vacuolated cytoplasm. Long cytoplasmic prolongations that join the zona pellucida are also present (Figure 1A; see also ref. [43]).

In the Jumonji 4-plex panels for ZZf females, the pyriform cells are extensively stained with KDM6B, weakly stained with JARID2 (Figure 2A). In the CaRe 4-plex panel the pyriform cells are extensively stained with CIRBP, with some weak staining for RelA and H3K4me3 in the nucleus (Figure 2B). In ZZf and ZWf females in both panels, the small and intermediate cells are stained almost exclusively with H3K4me3 (Figures 2 and 3). JARID2 (Figures 2A and 3A) and RelA (Figures 2B and 3B) show similar staining patterns in both ZWf and ZZf females; both are weakly dispersed throughout the theca and granulosa layers. H3K27me3 staining is very minimal and restricted to the theca in both females in each panel (Figures 2 and 3).

Testicular morphology

In the ZZm males of *P. vitticeps*, no mature sperm are present given the samples were collected following the breeding season. Some elongating spermatids are present, as are some spermatocytes and Sertoli cells. In both panels, H3K4me3 was extensively stained in the Sertoli cells and spermatocytes, whereas H3K27me3 was minimally stained (Figure 4). In the Jumonji 4-plex panel, KDM6B was abundantly expressed within the cell junctions that form near the basement membrane of the seminiferous tubules (Figure 4A). CIRBP staining was also abundant within the cell junctions, and also within the interstitial space (Figure 4B). JARID2 staining was weakly dispersed throughout the seminiferous tubules, a similar pattern to what was observed for RelA staining in the CaRe 4-plex panel (Figure 4).

Protein enrichment

The level of protein expression was determined by calculating the MIFI values for each antibody within a tissue at

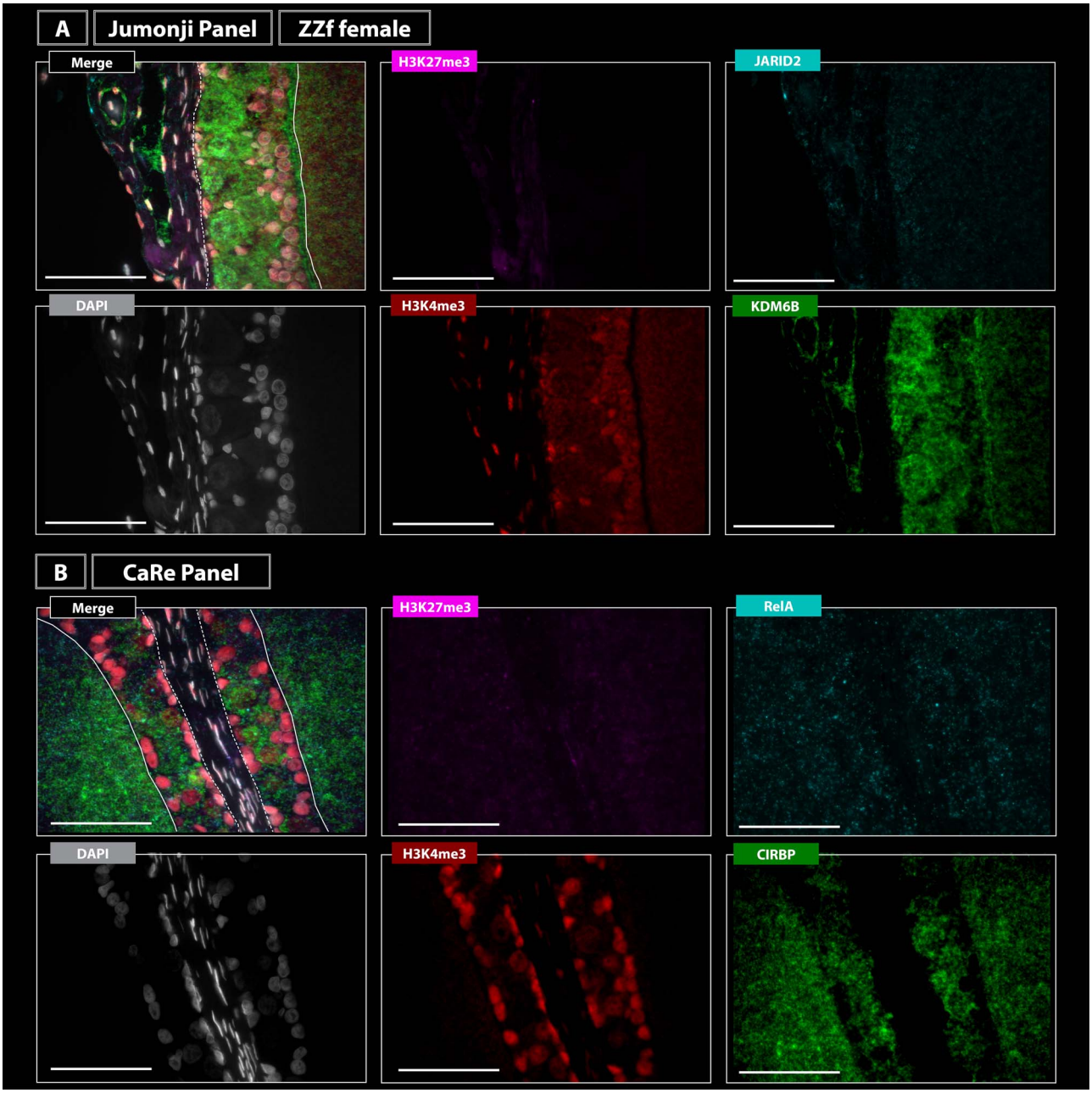

Figure 2. Immunofluorescence from two staining panels (Jumonji and CaRe panels) at 100× magnification in a ZZf sex reversed *Pogona vitticeps* female oocyte. The Jumonji panel shows staining of H3K27me3 (magenta), JARID2 (cyan), H4K4me3 (red), and KDM6B (green). H3K27me3 and JARID2 are weakly stained, while H3K4me3 and KDM6B are strongly stained in the theca and granulosa layer. The Care panel shows staining of H3K27me3 (magenta), RelA (cyan), H4K4me3 (red), and CIRBP (green). H3K27me3 and RelA are weakly stained, while H3K4me3 and CIRBP are strongly stained in the theca and granulosa layer. The dashed white line indicates the boundary between the theca (outermost layer) with the granulosa layer, and the solid white line demarcates the granulosa layer and the inside of the oocyte. Scale bar = 10 μm.

100× magnification using an automated imaging system. See "Materials and methods" for full details on how this analysis was conducted. As JARID2 staining was low in all tissues, it was not included in the protein expression analysis.

In the Jumonji 3-plex panel (H3K27me3, H3K4me3, and KDM6B), global expression levels for H3K27me3 was significantly higher in ZZm males compared with ZZf females ($P < 0.0001$) but not with ZWf females ($P = 0.27$). H3K27me3 levels were significantly higher in ZWf females compared with ZZf females ($P < 0.005$). For cells positive only for H3K27me3, levels did not significantly differ between the three sex classes (Figure 5).

Global staining of KDM6B did not differ between ZZf and ZWf females ($P = 0.106$), but was significantly lower in males compared with both females ($P < 0.0001$ for both pairwise comparisons). Cells positive only for KDM6B differed only marginally between the two female groups ($P < 0.02$), whereas expression was significantly lower in ZZm males compared with both ZZf and ZWf females ($P < 0.0005$ and $P < 0.0001$ respectively; Figure 5).

Global expression of H3K4me3 was significantly different between all groups, as was expression in single positive cells. ZWf females had the highest global expression of H3K4me3, they had the lowest expression in single positive cells for

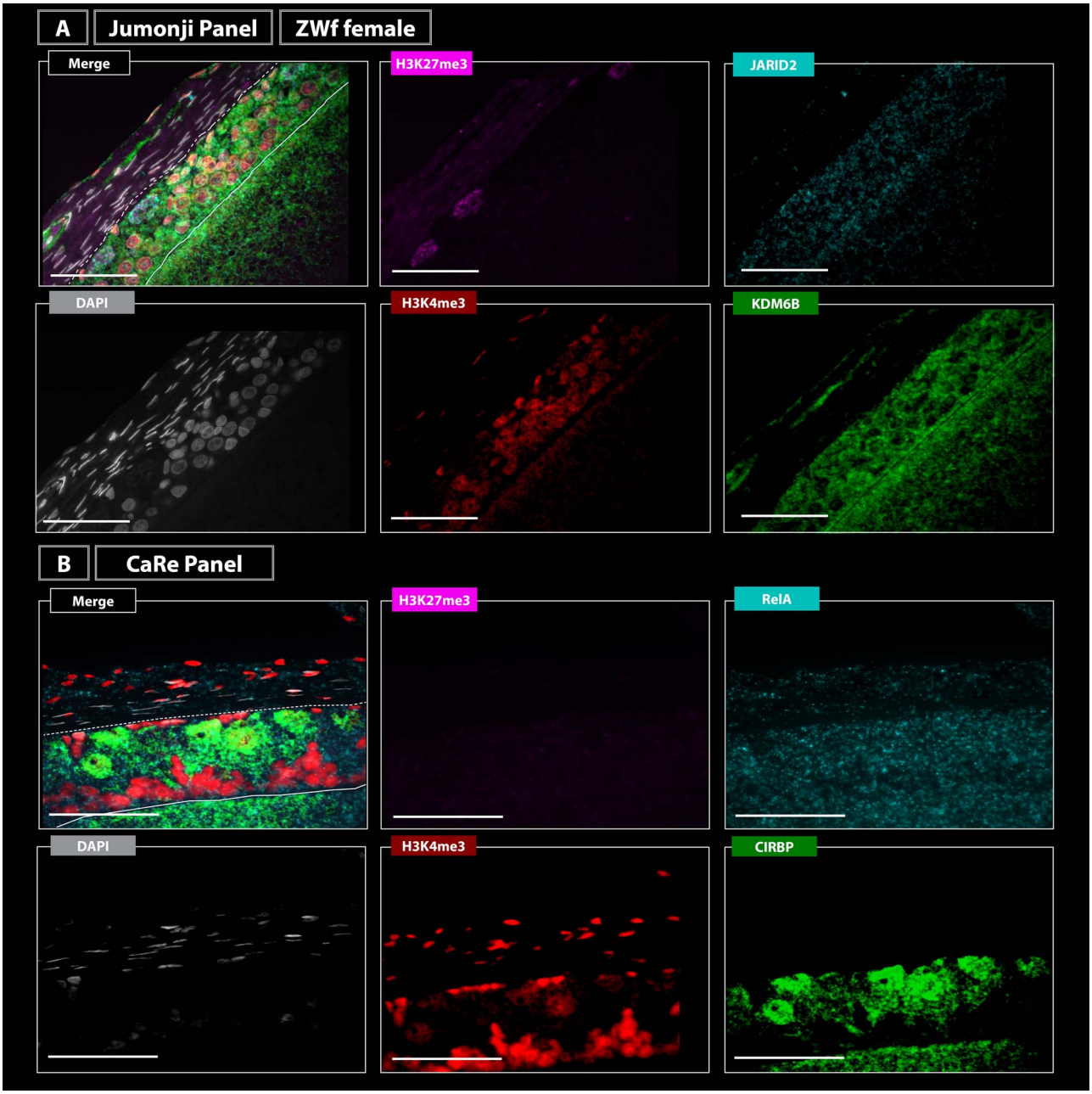

Figure 3. Immunofluorescence from two staining panels (Jumonji and CaRe panels) at 100× magnification in a ZWf concordant *Pogona vitticeps* female oocyte. The Jumonji panel shows staining of H3K27me3 (magenta), JARID2 (cyan), H4K4me3 (red), and KDM6B (green). H3K27me3 and JARID2 are weakly stained, while H3K4me3 and KDM6B are strongly stained in the theca and granulosa layer. The Care panel shows staining of H3K27me3 (magenta), RelA (cyan), H4K4me3 (red), and CIRBP (green). H3K27me3 and RelA are weakly stained, while H3K4me3 and CIRBP are strongly stained in the theca and granulosa layer. The dashed white line indicates the boundary between the theca (outermost layer) with the granulosa layer, and the solid white line demarcates the granulosa layer and the inside of the oocyte. Scale bar = 10 μm.

this mark, whereas the opposite was true for ZZm males (Figure 5).

Expression of KDM6B globally and in single positive cells was consistently lower in ZZm males compared with both ZZf and ZWf females. KDM6B was consistently higher in ZWf females compared with ZZf females. In contrast, expression patterns for the histone marks were not consistent between the sex classes and between global and single cell expression levels (Figure 5).

Four classes of cells positive for different combinations of the four targets were identified. Cells positive for H3K27me3 and KDM6B did not differ in expression between the three sex classes. The H3K27me3 and H3K4me3 class was not detected in ZWf females, but did not differ between ZZf females and ZZm males. Cells double positive for H3K4me3 and KDM6B were detected in the female classes, and not in males. Although the expression of H3K4me3 did not differ, expression of KDM6B was significantly higher in ZWf females compared with ZZf females. Cells triple positive for H3K27me3, H3K4me3, and KDM6B were only detected in females. Expression of H3K4me3 and KDM6B did not differ, however

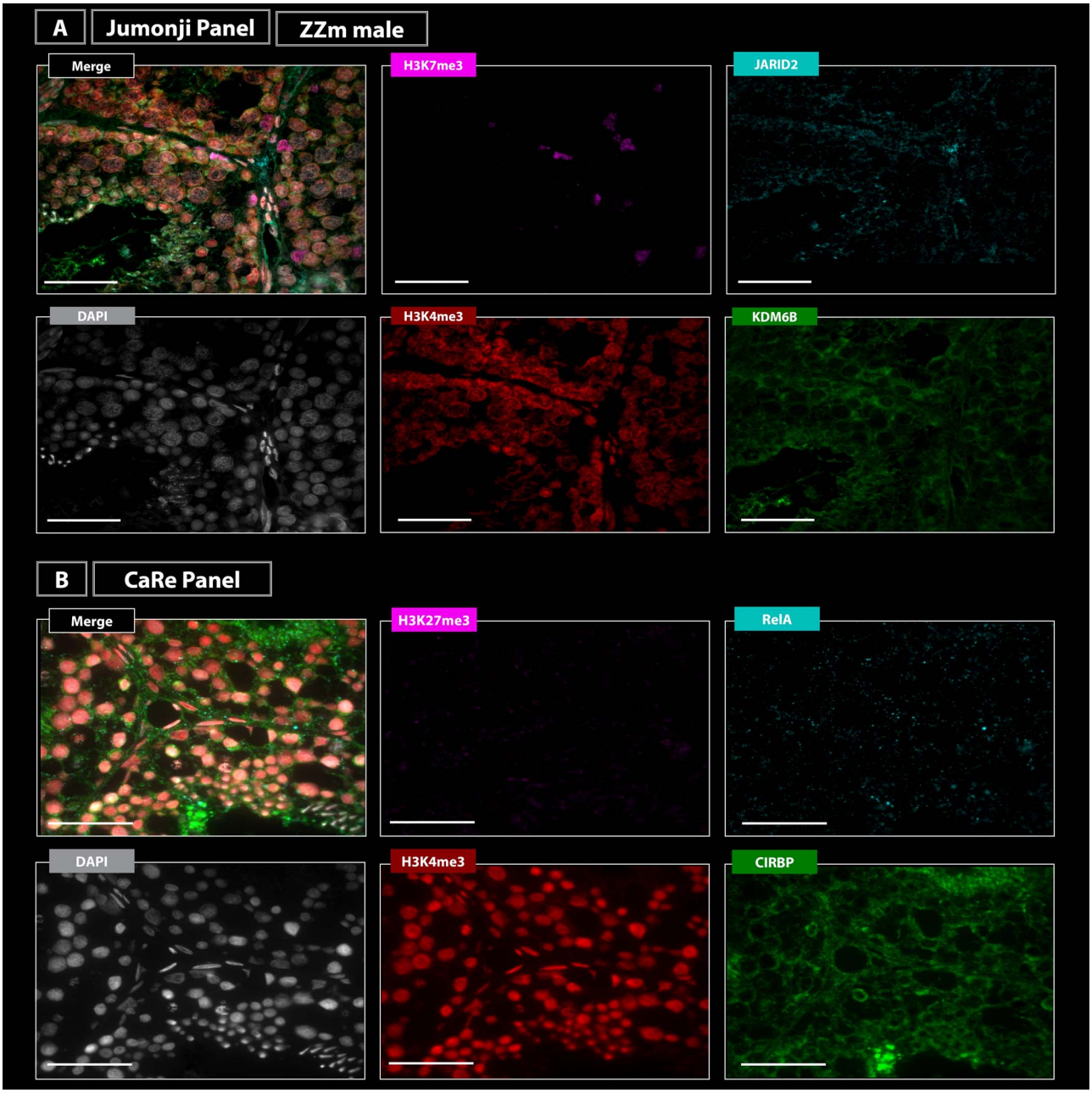

Figure 4. Immunofluorescence from two staining panels (Jumonji and CaRe panels) at 100× magnification in a ZZm male *Pogona vitticeps* testis. The Jumonji panel shows staining of H3K27me3 (magenta), JARID2 (cyan), H3K4me3 (red), and KDM6B (green). H3K27me3 and JARID2 are weakly stained, while H3K4me3 and KDM6B are strongly stained in the seminiferous tubules. The Care panel shows staining of H3K27me3 (magenta), RelA (cyan), H4K4me3 (red), and CIRBP (green). H3K27me3 and RelA are weakly stained, while H3K4me3 and CIRBP are strongly stained in the seminiferous tubules. Scale bar = 10 μm.

H3K27me3 was more highly expressed in ZWf females (Figure 5).

In the CaRe 4-plex panel global levels of CIRBP, RelA and H3K4me3 expression were significantly different between the three sex classes (Figure 6). CIRBP and H3K4me3 were highest in ZZf females, whereas RelA was highest in ZWf females. ZZm males exhibited the lowest expression of all targets. In all three sex classes, the only single positive cell class detected was for H3K4me3, which differed slightly between ZWf and ZZf females, but not between both female class and males. The only double positive class detected was H3K27me3 and CIRBP, which significantly differed between all sex classes, and both targets were highest in ZZf females. The only triple positive class was CIRBP, H3K4me3, and RelA, which differed significantly between the three sex classes. H3K4me3 and RelA were highest in ZZm males, whereas CIRBP was highest in ZZf females. Cells positive for all four targets were only detected in females, but levels did not differ between them (Figure 6).

It is important to note that while mean fluorescent intensity values for the protein targets can be assessed (summarized in Figure 7), the actual staining characteristics between the targets also needs to be considered visually. In all three sex classes in both the Jumonji and CaRe panels, H3K27me3 was very weakly stained, and in the CaRe panel RelA was weakly stained. This suggests that although differences in expression

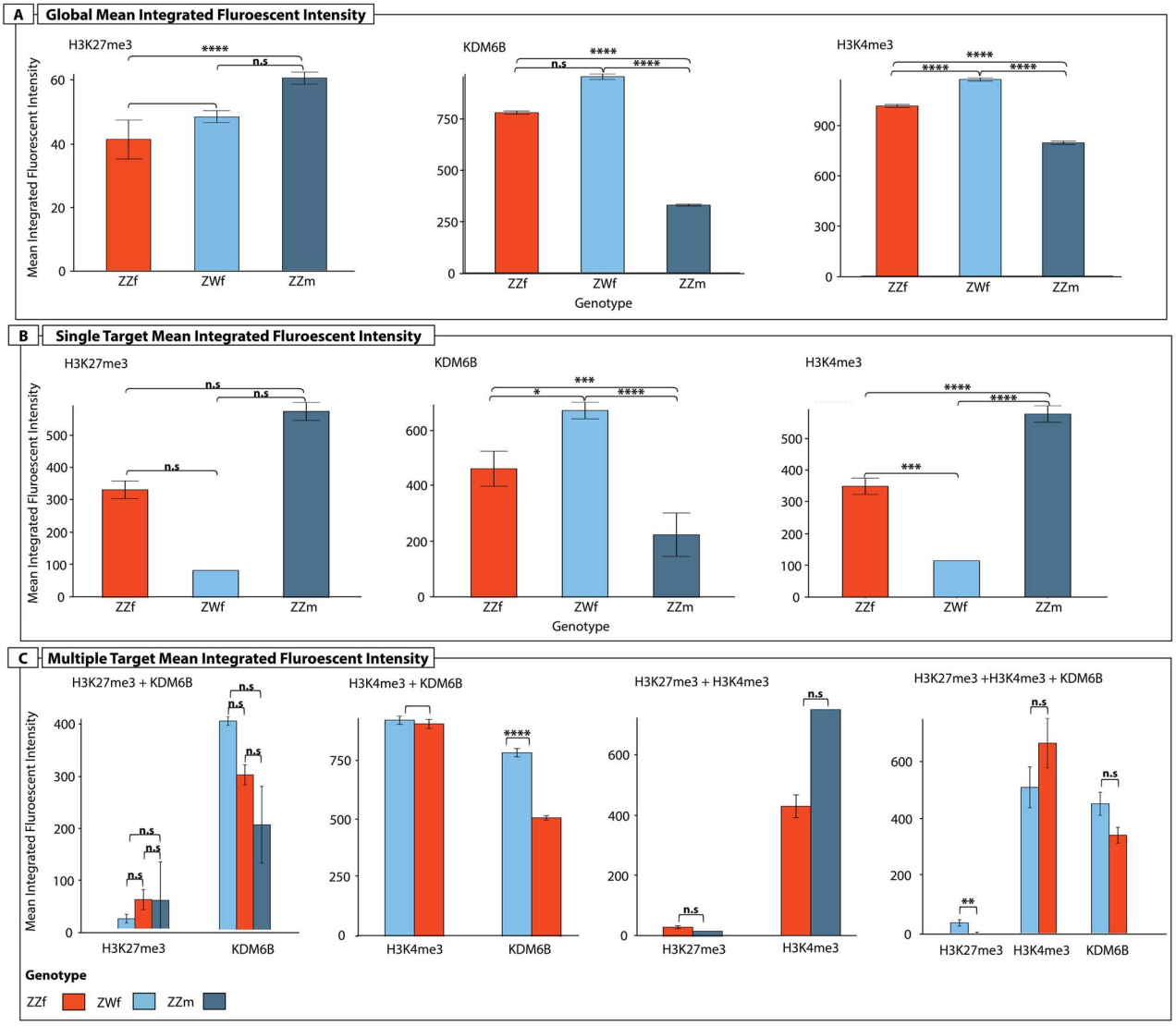

Figure 5. Mean integrated fluorescent intensity for the 3-plex Jumonji panel (H3K27me3, KDM6B, and H3K4me3) for protein enrichment (A) globally for a single target, (B) cells positive for only a single target, and (C) cells positive for multiple targets for each sex class in *Pogona vitticeps*: ZZf sex reversed females (red), ZWf concordant females (light blue), and ZZm males (dark blue). JARID2 was not included in this analysis due to low levels of staining. Analysis was conducted using a linear model, and significance (*P*-value) is denoted with asterisks (* < 0.05, ** < 0.01, *** < 0.001, **** < 0.0001, n.s. = not significant, $\alpha = 0.05$).

level was detected, the biological relevance of this is likely minimal.

Discussion

These data give insights to the protein dynamics in adult gonads of a squamate for the first time, and provides new understanding for reptiles more broadly, a vertebrate group for which there are few IHC data. The data for KDM6B, JARID2, RelA, and CIRBP are also novel for vertebrates more broadly, as these four proteins have been minimally studied in adult gonads even in mammalian model species. Taking both protein localization and expression information together, H3K4me3, KDM6B, and CIRBP emerge as particularly important proteins with roles in the functioning of both ovaries and testes.

KDM6B was consistently more highly expressed in ZWf females compared with ZZf females, however KDM6B was localized in the same regions of the granulosa layer between both females. High expression of KDM6B in ZWf females is not consistent with previously published RNA-seq data for *P. vitticeps*, which found *KDM6B* to be more highly expressed in ZZf females [17]. The reason for this discrepancy is unclear, though suggests that additional post-transcriptional regulation may occur in KDM6B. Future experiments are required to determine if there is consistency in these results, including proteomic sequencing. In both ZWf and ZZf females, KDM6B expression was strongest in the small and intermediate cells in the granulosa, with some staining in the pyriform cells of ZZf females. These cell types were also double positive for KDM6B and H3K4me3, a double mark that was not present in male cell types. Previous research on *P. vitticeps* has shown that *KDM6B* is highly expressed during sex reversal in embryonic development [7], a pattern that was also observed sex reversed adult females [17].

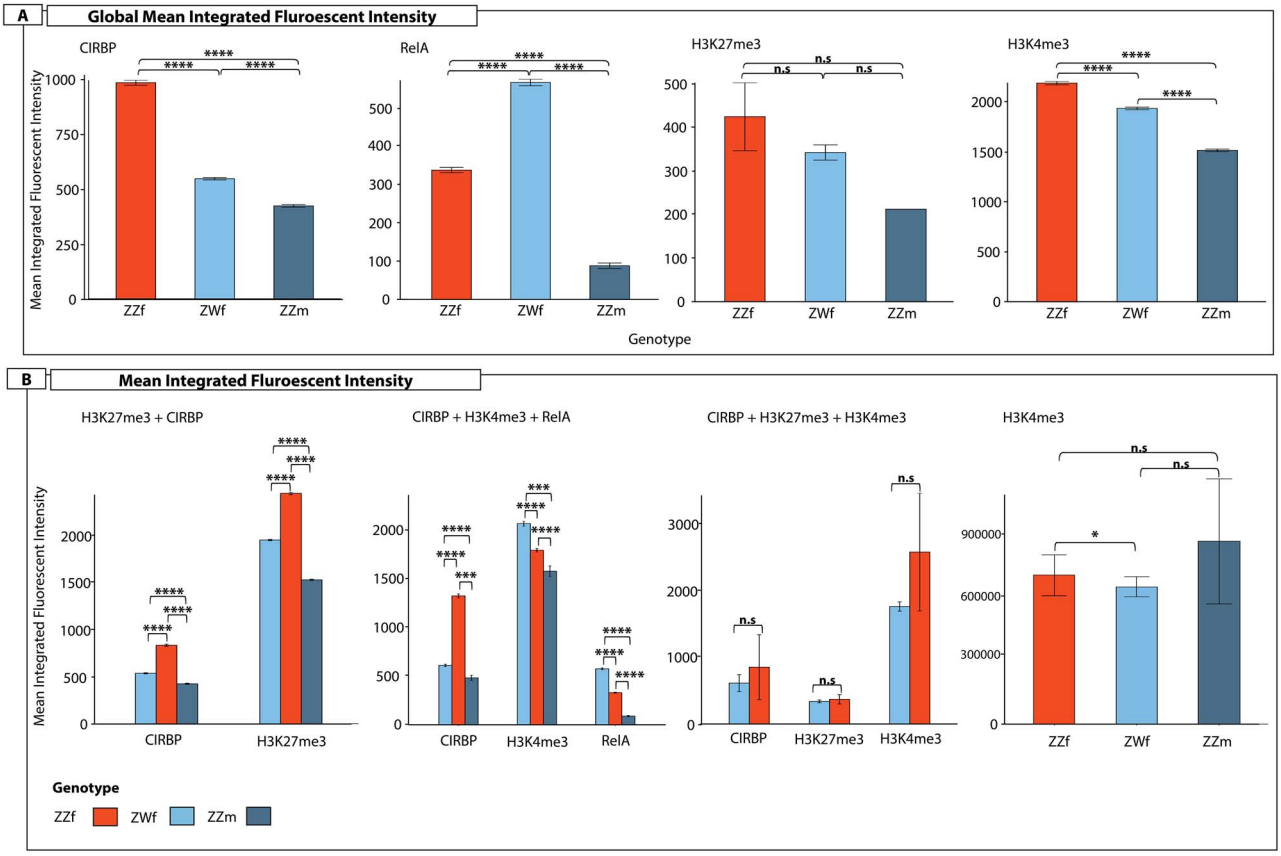

Figure 6. Mean integrated fluorescent intensity for (A) global or (B) grouped target expression for combinations of CIRBP, H3K27me3, RelA, and H3K4me3 for each sex class in *Pogona vitticeps*: ZZf sex reversed females (red), ZWf concordant females (light blue), and ZZm males (dark blue). Cells double positive for H3K4me3 and JARID2 were only detected in ZZm males. Analysis was conducted using a linear model, and significance (*P*-value) is denoted with asterisks (* < 0.05, ** < 0.01, *** < 0.001, **** < 0.0001, n.s = not significant, $\alpha = 0.05$).

H3K27me3 was weakly stained in both panels in all three sex classes. A possible explanation for the low levels of H3K27me3 is the prevalence of KDM6B, which demethylates H3K27me3 [21]. We also observed low levels of JARID2, which as a member of the PRC2 complex responsible for depositing H3K27me3 marks, may also be a contributing factor to the low levels of H3K27me3. These results suggest low levels of H3K27me3 and high levels of KDM6B are characteristic of adult *P. vitticeps* regardless of sex, however as fundamentally different organs, the localization of KDM6B differs between males and females. Previous work on adult gene expression in *P. vitticeps* found that *KDM6B* is more highly expressed in ZZf females than both ZWf females and ZZm males. An intron retention event in KDM6B genes was also observed in ZZf females, leading to the suggestion that the IR containing isoforms would not be translated into proteins [17]. The abundance of KDM6B staining observed in this study suggests the protein is translated, however future experiments are required to confirm whether or not the intron containing KDM6B isoform translated or not, and to determine the function of the resulting protein.

In the reptile granulosa, small cells are stem cells from which intermediate cells differentiate. Pyriform cells, which are a unique cell type to squamates, then differentiate from the intermediate cells [39, 44]. Both intermediate cells and pyriform cells have functions similar to gonadal nurse cells found in insect ovaries [45] as they support the growth of the oocyte by transferring organelles such as vesicles, Golgi, ribosomal bodies, mitochondria, and messenger and ribosomal RNAs into the ooplasm via intracellular bridges [46]. Given this function, it is unsurprising that a lysine demethylase like KDM6B and an active mark like H3K4me3 dominates in these cell types as opposed to those with repressive functions such as JARID2 and KDM6B.

Recent studies in mouse ovaries have shown that androgens target the catalytic subunit of the PRC2 complex, *EZH2*, which ultimately leads to reduced H3K27me3 methylation. At the same time, androgens also induce expression of *KDM6B*, which further serves to reduce levels of H3K27me3 in the ovaries [47]. Notably, cells in the *P. vitticeps* granulosa layer show an absence of H3K27me3, and an abundance of KDM6B, suggesting that this mechanism of ovarian gene regulation may be shared in *P. vitticeps*, and perhaps reptiles more broadly.

KDM6B is also abundantly expressed in the cell junctions within the seminiferous tubules in ZZm males, a localization pattern that was also shared with CIRBP. In two turtle species (*Pelodiscus sinensis* and *Pelodiscus maackii*), junction proteins CLDN11 and CX43, which have established functions in mammalian testes, showed highly similar localization patterns to those of KDM6B and CIRBP observed in *P. vitticeps* [48, 49]. Although further work is required, this suggests that KDM6B and CIRBP may have undescribed functions in the gap junctions of testes in *P. vitticeps*, and perhaps reptiles more broadly.

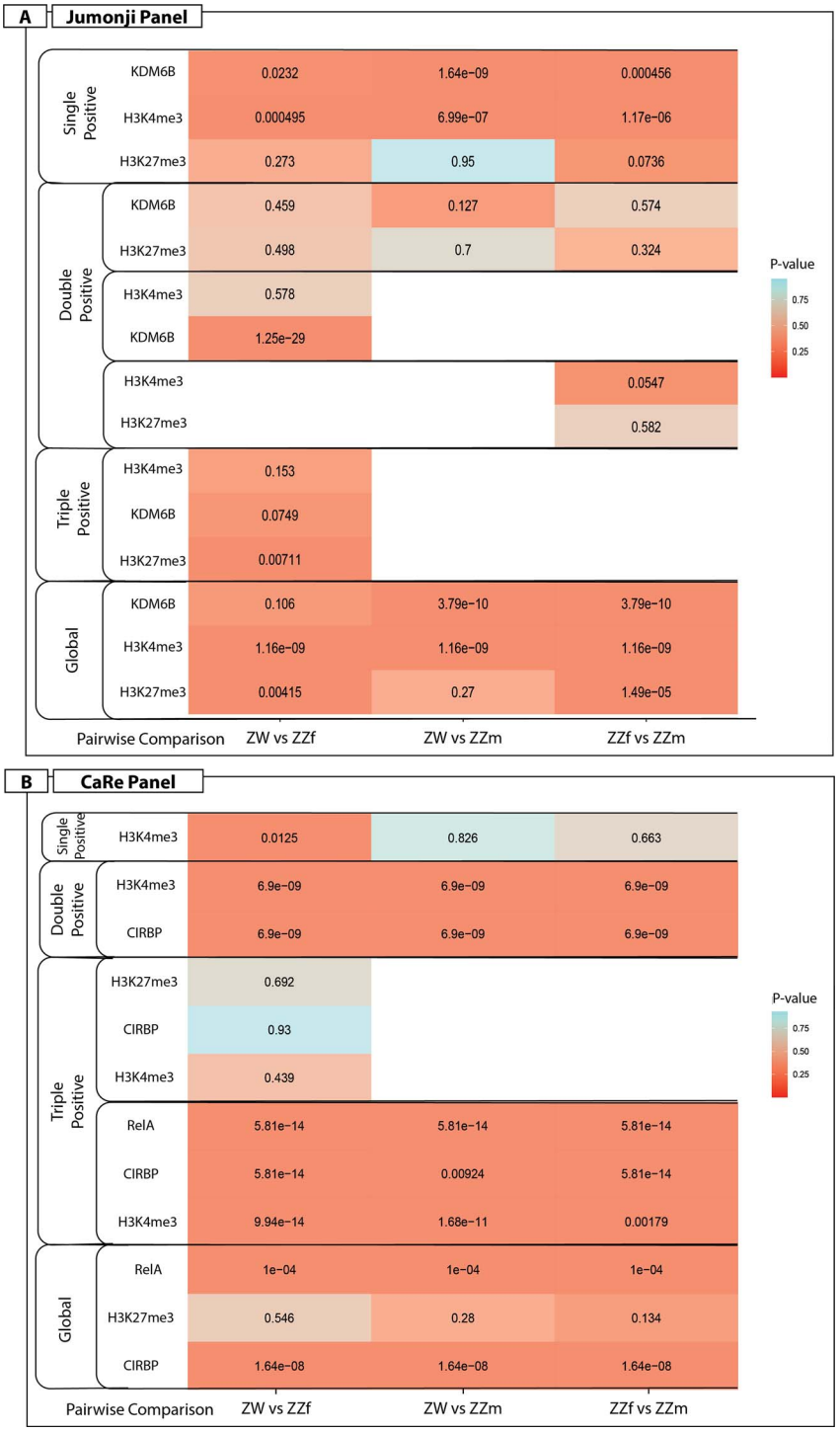

Figure 7. Heatmap showing a summary of all linear models conducted on mean integrate intensity values from the Jumonji (H3K27me3, H3K4me3, and KDM6B) and CaRe (H3K27me3, H3K4me3, CIRBP, and RelA) panels. *P*-values for each pairwise comparison (*x*-axis, ZW vs ZZf, ZW vs ZZm, and ZZf vs ZZm), for the staining classes are reported, and colored by significance: blue = not significant ($P \geq 0.05$), red = significant ($P \leq 0.05$). Single positive staining is defined by the population of cells detected by the ASI software to be positive for a single target, double positive indicates staining in a population of cells with combinations of two targets (listed on the *y*-axis), and triple positive staining indicates cells with combinations of three targets (listed on the *y*-axis). Global expression for each target is the total expression of the target in all cells detected, regardless of co-staining with other targets.

The functions of CIRBP in the ovarian granulosa under normal conditions are not well understood even in mammalian models. Its expression was associated with hypothermia in granulosa cell lines [28], and is more generally involved in the mammalian cold-shock response in other organs [50]. Its abundance in the granulosa of adult females and cell junctions in adult males of *P. vitticeps*, suggest an additional role for CIRBP that is not triggered by an environmental stressor, and relates more to normal functioning of the gonads. Immunostaining conducted on hatchlings of two turtle species

(*Caretta caretta* and *Dermochelys coriacea*) showed high levels of CIRBP protein expression in female gonads rather than male gonads [14]. In this case, it was suggested that CIRBP expression may be influenced by incubation temperature, as is often the case for this gene in many reptile species (reviewed in ref. [34]). In adult *P. vitticeps* this explanation seems unlikely, so further experimentation is required to determine the role of CIRBP in adult gonads, and roles it may have in reptiles more broadly.

Methylation dynamics during germ cell development have been extensively characterized in mammals. H3K27me3 and H3K4me3 are associated with bivalent chromatin, and are commonly observed during spermatogenesis and oogenesis [51–53]. In *P. vitticeps,* all three sex classes exhibited abundant expression of H3K4me3 and minimal expression of H3K27me3, suggesting a lack of bivalent chromatin in both ovaries and testes. Given the samples were collected following the breeding season, these data likely capture a more latent reproductive stage, and during a more active reproductive period the dynamics of these methylation marks would likely be different. Future exploration of these methylation marks during embryonic development would give more specific insights to their role, and in particular how their abundance may change due to different incubation temperatures. Combining immunostaining data with other methods for assessing methylation, such as chromatin immunoprecipitation sequencing (ChIP-seq) of H3K27me3 and H3K4me3, would also be a powerful approach to understand the regions of the genome targeted with these marks.

Now that effective staining of these targets has been established in *P. vitticeps*, an important avenue for future research is to assess the dynamics of these proteins during embryonic development. Previous research on sex reversal during embryogenesis in *P. vitticeps* has implicated *JARID2*, *KDM6B*, and *CIRBP* as playing a crucial role in temperature responses and gene regulation changes [7, 34]. We expect that the immunostaining characteristics between adults and embryos will be considerably different, particularly when the embryos are exposed to sex reversal inducing temperatures. For example, although CIRBP has been shown to be highly upregulated in *P. vitticeps* and other species with temperature dependent sex determination [19, 27], its function is unknown. Research in mammalian systems has demonstrated that extreme temperatures cause CIRBP to translocate from the nucleus to the cytoplasm where it can stabilize mRNA transcripts [50, 54]. Immunostaining of CIRBP in *P. vitticeps* embryos undergoing sex reversal would reveal whether this occurs, improving understanding of mechanisms involved in temperature response, and that these mechanisms are shared across divergent vertebrate lineages.

Research on non-model organisms, and particularly in non-mammalian systems, presents many challenges. We have shown the advantages that can be gained by looking to techniques available in biomedical research, and using them for novel applications in new systems. We believe that this is the first immunostaining data to be generated for a non-mammalian species using advanced automated staining equipment and computer aided cell analysis. A significant barrier for many would be the costs associated with these types of automated systems, and potential difficulties obtaining antibodies with sufficiently how homology and good cross-reactivity. However there are major advantages to be gained as automation improves accuracy and reproducibility of staining and interpretation.

These data give not only important new insights into the protein dynamics of these targets, but also provides a crucial foundation for future research. Confirmation that mammalian antibodies cross react in *P. vitticeps* paves the way for experiments that can take advantage of this new immunohistochemical resource to gain a new understanding of the role of these proteins during embryonic development, and most importantly for *P. vitticeps*, the molecular underpinnings of sex reversal.

Supplementary material

Supplementary material is available at *BIOLRE* online.

Author contributions

S.L.W. collected and prepared the tissues, selected antibodies, assisted with imaging protocols, conducted all analysis, prepared all figures, and the manuscript. R.M. conducted staining and imaging protocols, and assisted with image preparation and analysis. C.E.H., S.R., and A.G. conceived of the study and made available the required resources. All authors contributed to the writing of the manuscript.

Acknowledgments

We thank Jin Dai for his contributions to optimizing the staining protocols. We thank Dr Wendy Ruscoe and Jacqui Richardson for their animal husbandry expertise. We also thank Dr Craig Smith for providing feedback on this manuscript. We thank the Histology Services at QIMR for their support in this project for our tissue processing, in particular we thank the assistance of Andrew Masel and Clay Winterford.

Data availability

The data underlying this article will be shared on reasonable request to the corresponding author.

Conflict of interest

The authors declare they have no conflicts of interest.

References

1. Sarre SD, Georges A, Quinn A. The ends of a continuum: genetic and temperature-dependent sex determination in reptiles. *Bio Essays* 2004; **26**:639–645.
2. Whiteley SL, Castelli MA, Dissanayake DS, Holleley CE, Georges A. Temperature-induced sex reversal in reptiles: prevalence, discovery, and evolutionary implications. *Sex Dev* 2021; **15**:148–156.
3. Ezaz T, Quinn AE, Miura I, Sarre SD, Georges A, Marshall Graves JA. The dragon lizard *Pogona vitticeps* has ZZ/ZW micro-sex chromosomes. *Chromosome Res* 2005; **13**:763–776.
4. Quinn AE, Georges A, Sarre SD, Guarino F, Ezaz T, Marshall Graves JA. Temperature sex reversal implies sex gene dosage in a reptile. *Science* 2007; **316**:411.
5. Li H, Holleley CE, Elphick M, Georges A, Shine R. The behavioural consequences of sex reversal in dragons. *Proc R Soc B Biol Sci* 2016; **283**:1–7.
6. Holleley CE, O'Meally D, Sarre SD, Marshall Graves JA, Ezaz T, Matsubara K, Azad B, Zhang X, Georges A. Sex reversal triggers the rapid transition from genetic to temperature-dependent sex. *Nature* 2015; **523**:79–82.

7. Whiteley SL, Holleley CE, Blackburn J, Deveson IW, Wagner S, Marshall Graves JA, Georges A. Two transcriptionally disctinct pathways drive female development in a reptile with temperature induced sex reversal. *PLoS Genet* 2021; **17**:e1009465.
8. Jones MEH, Pistevos JCA, Cooper N, Lappin AK, Georges A, Hutchinson MN, Holleley CE. Reproductive phenotype predicts adult bite-force performance in sex-reversed dragons (*Pogona vitticeps*). *J Exp Zool Part A Ecol Integr Physiol* 2020; **333**:252–263.
9. Amer SAM, Kumazawa Y. Mitochondrial genome of *Pogona vitticepes* (Reptilia; Agamidae): control region duplication and the origin of Australasian agamids. *Gene* 2005; **346**:249–256.
10. Deakin JE, Edwards MJ, Patel H, O'Meally D, Lian J, Stenhouse R, Ryan S, Livernois AM, Azad B, Holleley CE, Li Q, Georges A. Anchoring genome sequence to chromosomes of the central bearded dragon (*Pogona vitticeps*) enables reconstruction of ancestral squamate macrochromosomes and identifies sequence content of the Z chromosome. *BMC Genomics* 2016; **17**:447.
11. Georges A, Li Q, Lian J, O'Meally D, Deakin J, Wang Z, Zhang P, Fujita M, Patel HR, Holleley CE, Zhou Y, Zhang X *et al.* High-coverage sequencing and annotated assembly of the genome of the Australian dragon lizard *Pogona vitticeps*. *Gigascience* 2015; **4**:45.
12. Maurizii MG, Cavaliere V, Gamberi C, Lasko P, Gargiulo G, Taddei C. Vasa protein is localized in the germ cells and in the oocyte-associated pyriform follicle cells during early oogenesis in the lizard *Podarcis sicula*. *Dev Genes Evol* 2009; **219**:361–367.
13. Machado-Santos C, Santana LN D S, Vargas RF, Abidu-Figueiredo M, de Brito-Gitirana L, Chagas MA. Histological and immunohistochemical study of the ovaries and oviducts of the juvenile female of *Caiman latirostris* (Crocodilia: Alligatoridae). *Fortschr Zool* 2015; **32**:395–402.
14. Tezak BM, Guthrie K, Wyneken J. An Immunohistochemical approach to identify the sex of young marine turtles. *Anat Rec* 2017; **300**:1512–1518.
15. Wyneken J. Reptilian renal structure and function. *Proc Assoc Reptil Amphib Vet* 2013; **41**:72–78.
16. Sarı F, Kaska Y. Histochemical and immunohistochemical studies of the gonads and paramesonephric ducts of male and female hatchlings of loggerhead sea turtles (*Caretta caretta*). *Biotech Histochem* 2016; **91**:428–437.
17. Deveson IW, Holleley CE, Blackburn J, Marshall Graves JA, Mattick JS, Waters PD, Georges A. Differential intron retention in Jumonji chromatin modifier genes is implicated in reptile temperature-dependent sex determination. *Sci Adv* 2017; **3**:e1700731.
18. Ge C, Ye J, Weber C, Sun W, Zhang H, Zhou Y, Cai C, Qian G, Capel B. The histone demethylase KDM6B regulates temperature-dependent sex determination in a turtle species. *Science* 2018; **360**: 645–648.
19. Schroeder AL, Metzger KJ, Miller A, Rhen T. A novel candidate gene for temperature-dependent sex determination in the common snapping turtle. *Genetics* 2016; **203**:557–571.
20. Sanulli S, Justin N, Teissandier A, Ancelin K, Portoso M, Caron M, Michaud A, Lombard B, da Rocha ST, Offer J, Loew D, Servant N *et al.* Jarid2 methylation via the PRC2 complex regulates H3K27me3 deposition during cell differentiation. *Mol Cell* 2015; **57**:769–783.
21. Xiang Y, Zhu Z, Han G, Lin H, Xu L, Chen CD. JMJD3 is a histone H3K27 demethylase. *Cell Res* 2007; **17**:850–857.
22. Nakajima R, Okano H, Noce T. JMJD1C exhibits multiple functions in epigenetic regulation during spermatogenesis. *PLoS One* 2016; **11**:1–22.
23. Kuroki S, Akiyoshi M, Tokura M, Miyachi H, Nakai Y, Kimura H, Shinkai Y, Tachibana M. JMJD1C, a jmjc domain-containing protein, is required for long-term maintenance of male germ cells in mice. *Biol Reprod* 2013; **89**:1–9.
24. Godmann M, Auger V, Ferraroni-Aguiar V, Di Sauro A, Sette C, Behr R, Kimmins S. Dynamic regulation of histone H3 methylation at lysine 4 in mammalian spermatogenesis. *Biol Reprod* 2007; **77**: 754–764.
25. Lesch BJ, Page DC. Poised chromatin in the mammalian germ line. *Development* 2014; **141**:3619–3626.
26. Rhen T, Schroeder A. Molecular mechanisms of sex determination in reptiles. *Sex Dev* 2010; **4**:16–28.
27. Haltenhof T, Kotte A, de Bortoli F, Schiefer S, Meinke S, Emmerichs A-K, Petermann KK, Timmermann B, Franz A, Wahl M, Imhof P, Preussner M *et al.* A conserved kinase-based body temperature sensor globally controls alternative splicing and gene expression. *Mol Cell* 2020; **78**:1–13.
28. Kun Y, Qian Z, GuYue L, YangYang P, SiJiu Y, Jun Feng H, Yan C. Effects of mild cold shock followed by warming up at 37°C on the ovarian granulosa cellular stress response of the yak. *Acta Vet Zootech Sin* 2015; **46**:738–745.
29. Rao M, Ke D, Cheng G, Hu S, Wu Y, Wang Y, Zhou F, Liu H, Zhu C, Xia W. The regulation of CIRBP by transforming growth factor beta during heat shock-induced testicular injury. *Andrology* 2019; **7**:244–250.
30. Yeung F, Hoberg JE, Ramsey CS, Keller MD, Jones DR, Frye RA, Mayo MW. Modulation of NF-κB-dependent transcription and cell survival by the SIRT1 deacetylase. *EMBO J* 2004; **23**:2369 LP – 2380.
31. Teo H, Ghosh S, Luesch H, Ghosh A, Wong ET, Malik N, Orth A, De Jesus P, Perry AS, Oliver JD, Tran NL, Speiser LJ *et al.* Telomere-independent Rap1 is an IKK adaptor and regulates NF-κB-dependent gene expression. *Nat Cell Biol* 2010; **12**:758–767.
32. Nakshatri H, Appaiah HN, Anjanappa M, Gilley D, Tanaka H, Badve S, Crooks PA, Mathews W, Sweeney C, Bhat-Nakshatri P. Nf-kB-dependent and -independent epigenetic modulation using the novel anti-cancer agent DMAPT. *Cell Death Dis* 2015; **6**:e1608.
33. Pavlová S, Klucska K, Vašíček D, Ryban L, Harrath AH, Alwasel SH, Sirotkin AV. The involvement of SIRT1 and transcription factor NF-κB (p50/p65) in regulation of porcine ovarian cell function. *Anim Reprod Sci* 2013; **140**:180–188.
34. Castelli MA, Whiteley SL, Georges A, Holleley CE. Cellular calcium and redox regulation: the mediator of vertebrate environmental sex determination? *Biol Rev* 2020; **95**:680–695.
35. Tu WJ, McCuaig RD, Melino M, Rawle DJ, Le TT, Yan K, Suhrbier A, Johnston RL, Koufariotis LT, Waddell N, Cross EM, Tsimbalyuk S *et al.* Targeting novel LSD1-dependent ACE2 demethylation domains inhibits SARS-CoV-2 replication. *Cell Discov* 2021; **7**.
36. Tu WJ, McCuaig RD, Tan AHY, Hardy K, Seddiki N, Ali S, Dahlstrom JE, Bean EG, Dunn J, Forwood J, Tsimbalyuk S, Smith K *et al.* Targeting nuclear LSD1 to reprogram cancer cells and reinvigorate exhausted T cells via a novel LSD1-EOMES switch. *Front Immunol* 2020; **11**:1–23.
37. Schindelin J, Arganda-Carreras I, Frise E, Kaynig V, Longair M, Pietzsch T, Preibisch S, Rueden C, Saalfeld S, Schmid B, Tinevez JY, White DJ *et al.* Fiji: An open-source platform for biological-image analysis. *Nat Methods* 2012; **9**:676–682.
38. Wickham H. *ggplot2: Elegant Graphics for Data Analysis*. New York: Springer; 2016.
39. Vieira S, de Pérez GR, Ramírez-Pinilla MP. Ultrastructure of the ovarian follicles in the placentotrophic Andean lizard of the genus Mabuya (Squamata: Scincidae). *J Morphol* 2010; **271**:738–749.
40. Da SD, Cassel M, Mehanna M, Ferreira A, Dolder MAH. Follicular development and reproductive characteristics in four species of Brazilian Tropidurus lizards. *Zoolog Sci* 2018; **35**:553–563.
41. Prisco M, Valiante S, Romano M, Ricchiari L, Liguoro A, Laforgia V, Limatola E, Andreuccetti P. Ovarian follicle cells in *Torpedo marmorata* synthesize vitellogenin. *Mol Reprod Dev* 2004; **67**: 424–429.
42. Raucci F, Di Fiore MM. The maturation of oocyte follicular epithelium of *Podarcis s. sicula* is promoted by D-aspartic acid. *J Histochem Cytochem* 2010; **58**:157–171.
43. Uribe MDCA, Omana MEM, Quintero JG, Guillette LJ. Seasonal variation in ovarian histology of the viviparous lizard *Sceloporus torquatus torquatus*. *J Morphol* 1995; **226**:103–119.

44. Lozano A, Ramírez-Bautista A, Uribe MC. Oogenesis and ovarian histology in two populations of the viviparous lizard *Sceloporus grammicus* (Squamata: Phrynosomatidae) from the central Mexican Plateau. *J Morphol* 2014; **275**: 949–960.
45. Tammaro S, Simoniello P, Filosa S, Motta CM. Block of mitochondrial apoptotic pathways in lizard ovarian follicle cells as an adaptation to their nurse function. *Cell Tissue Res* 2007; **327**: 625–635.
46. Motta CM, Scanderbeg MC, Filosa S, Andreuccetti P. Role of pyriform cells during the growth of oocytes in the lizard *Podarcis sicula*. *J Exp Zool* 1995; **273**:247–256.
47. Roy S, Huang B, Sinha N, Wang J, Sen A. Androgens regulate ovarian gene expression by balancing Ezh2-Jmjd3 mediated H3K27me3 dynamics. *PLoS Genet* 2021; **17**: 1–21.
48. Ahmed N, Yang P, Chen H, Ujjan IA, Haseeb A, Wang L, Soomro F, Faraz S, Sahito B, Ali W, Chen Q. Characterization of inter-Sertoli cell tight and gap junctions in the testis of turtle: protect the developing germ cells from an immune response. *Microb Pathog* 2018; **123**:60–67.
49. Park CJ, Ha CM, Lee JE, Gye MC. Claudin 11 inter-sertoli tight junctions in the testis of the Korean soft-shelled turtle (*Pelodiscus maackii*). *Biol Reprod* 2015; **92**:1–13.
50. Zhong P, Huang H. Recent progress in the research of cold-inducible RNA-binding protein. *Furture Sci OA* 2017; **3**:FSO246.
51. Bonnet-Garnier A, Feuerstein P, Chebrout M, Fleurot R, Jan HU, Debey P, Beaujean N. Genome organization and epigenetic marks in mouse germinal vesicle oocytes. *Int J Dev Biol* 2012; **56**: 877–887.
52. Zhang L, Wang J, Pan Y, Jin J, Sang J, Huang P, Shao G. Expression of histone H3 lysine 4 methylation and its demethylases in the developing mouse testis. *Cell Tissue Res* 2014; **358**: 875–883.
53. An J, Qin J, Wan Y, Zhang Y, Hu Y, Zhang C, Zeng W. Histone lysine methylation exhibits a distinct distribution during spermatogenesis in pigs. *Theriogenology* 2015; **84**:1455–1462.
54. De Leeuw F, Zhang T, Wauquier C, Huez G, Kruys V, Gueydan C. The cold-inducible RNA-binding protein migrates from the nucleus to cytoplasmic stress granules by a methylation-dependent mechanism and acts as a translational repressor. *Exp Cell Res* 2007; **313**:4130–4144.